ARTICLES

# Bone progenitor dysfunction induces myelodysplasia and secondary leukaemia

Marc H. G. P. Raaijmakers[1,6,7]*, Siddhartha Mukherjee[1,2,6,7]*†, Shangqin Guo[1,6,7], Siyi Zhang[1,6,7], Tatsuya Kobayashi[3], Jesse A. Schoonmaker[1,6,7], Benjamin L. Ebert[8,9], Fatima Al-Shahrour[8,9], Robert P. Hasserjian[4], Edward O. Scadden[1,6,7], Zinmar Aung[1,6,7], Marc Matza[1,6,7], Matthias Merkenschlager[10], Charles Lin[5], Johanna M. Rommens[11] & David. T. Scadden[1,2,6,7]

**Mesenchymal cells contribute to the 'stroma' of most normal and malignant tissues, with specific mesenchymal cells participating in the regulatory niches of stem cells. By examining how mesenchymal osteolineage cells modulate haematopoiesis, here we show that deletion of *Dicer1* specifically in mouse osteoprogenitors, but not in mature osteoblasts, disrupts the integrity of haematopoiesis. Myelodysplasia resulted and acute myelogenous leukaemia emerged that had acquired several genetic abnormalities while having intact *Dicer1*. Examining gene expression altered in osteoprogenitors as a result of *Dicer1* deletion showed reduced expression of *Sbds*, the gene mutated in Schwachman–Bodian–Diamond syndrome—a human bone marrow failure and leukaemia pre-disposition condition. Deletion of *Sbds* in mouse osteoprogenitors induced bone marrow dysfunction with myelodysplasia. Therefore, perturbation of specific mesenchymal subsets of stromal cells can disorder differentiation, proliferation and apoptosis of heterologous cells, and disrupt tissue homeostasis. Furthermore, primary stromal dysfunction can result in secondary neoplastic disease, supporting the concept of niche-induced oncogenesis.**

Mesenchymal cells are a part of virtually every tissue in metazoans, and are thought to participate in organ formation, cellular composition, patterning and size. In adult tissues, these cells are considered stroma without clear function. Identification of somatic stem cell populations has made the study of heterologous cells comprising their niche possible. Mesenchymal cells of osteolineage have been shown to regulate haematopoietic stem cells (HSC)[1,2], with *osterix* (also known as *Sp7*)-expressing skeletal progenitors initiating ectopic HSC niche formation[3]. We previously examined mesenchymal–HSC interactions using mice engineered to express individual genes in osteoblastic cells[1,4], and now sought to define more precisely the stage of osteolineage differentiation critical for haematopoiesis using promoters more restricted in their expression to alter candidate genes. We chose to alter a gene that could modulate a landscape of other gene products.

*Dicer1* is an RNase III endonuclease essential for microRNA (miRNA) biogenesis[5] and RNA processing[6]. miRNAs regulate haematopoietic cell fate[7], and their global downregulation by *Dicer1* deletion promotes tumorigenesis in a cancer-cell-autonomous manner[8]. We used *Dicer1* deletion as a means of altering several gene products in subsets of mesenchymal osteolineage cells. We intercrossed mice expressing green fluorescent protein (GFP)-Cre recombinase under the transcriptional control of the *osterix*[9] promoter expressed in osteoprogenitor cells to mice with floxed *Dicer1* alleles[10], generating Osx-GFP-Cre$^{+}$ Dicer$^{fl/+}$ (OCD$^{fl/+}$control) and Osx-GFP-Cre$^{+}$ Dicer$^{fl/fl}$ (OCD$^{fl/fl}$ mutant) mice. The Cre transgene in this model is expressed coordinately with endogenous osterix[11] (Fig. 1a). Mutant mice were born at Mendelian frequency, but showed growth retardation and impaired survival (~30% mutant mortality by 8 weeks). Therefore, we examined mice at 4–6 weeks of age.

## Impaired osteoblastic differentiation

*Dicer1* gene deletion in bone was shown by genomic PCR (Fig. 1b) and its efficiency confirmed by quantitative PCR of *Dicer1* messenger RNA in primary GFP$^{+}$ (CD45$^{-}$lineage$^{-}$CD31$^{-}$) cells (Fig. 1c, d and Supplementary Fig. 1a, b). Dicer1 was not deleted in haematopoietic stem and progenitor cells (Fig. 1e) nor in other haematopoietic subpopulations (not shown). Bone marrow stromal osteogenic colony number was decreased relative to total colony forming number (colony-forming unit alkaline phosphatase (CFU-ALK)/CFU-fibroblast (CFU-F)), indicative of reduced osteogenic differentiation (Fig. 1f, g). OCD$^{fl/fl}$ bone marrow stromal cultures also demonstrated decreased alkaline phosphatase and calcified matrix deposition after osteogenic differentiation (Supplementary Fig. 1d). *In vivo*, osteoblasts from OCD$^{fl/fl}$ mice expressed less of the terminal differentiation marker *osteocalcin* (also known as *Bglap*) (Fig. 1h and Supplementary Fig. 1e). Altered texture of the mineralized bone matrix was observed (Supplementary Fig. 1f), but not reduction in trabecular or cortical bone volume (Supplementary Fig. 1g, h). Osteoblast number was modestly, although significantly, decreased, whereas osteoclast number and function were not affected (Supplementary Fig. 1i–k and data not shown). Taken together, the data show that *Dicer1* deletion in osteoprogenitors impairs osteoblastic differentiation both *in vitro* and *in vivo*.

[1]Center for Regenerative Medicine, Massachusetts General Hospital and Harvard Medical School CPZN, Room 4265A, 185 Cambridge Street, [2]Cancer Center, Massachusetts General Hospital, [3]Endocrine Unit, Massachusetts General Hospital and Harvard Medical School, [4]Department of Pathology, Massachusetts General Hospital and Harvard Medical School, [5]Wellman Center for Photomedicine, Massachusetts General Hospital and Harvard Medical School, Boston, Massachusetts 02114, USA. [6]Department of Stem Cell and Regenerative Biology, Harvard University, [7]Harvard Stem Cell Institute, [8]Broad Institute, Cambridge, Massachusetts 02138, USA. [9]Hematology Division, Brigham and Women's Hospital, Boston, Massachusetts 02115, USA. [10]Lymphocyte Development Group, Medical Research Council Clinical Sciences Centre, Imperial College London, Du Cane Road, London W12 0NN, UK. [11]Program in Genetics and Genome Biology, The Hospital for Sick Children, Department of Molecular Genetics, University of Toronto, Toronto, Ontario M5S 1A8, Canada. †Present address: Department of Medicine and Irving Cancer Research Center, Columbia University School of Medicine, New York 10032, USA.
*These authors contributed equally to this work.

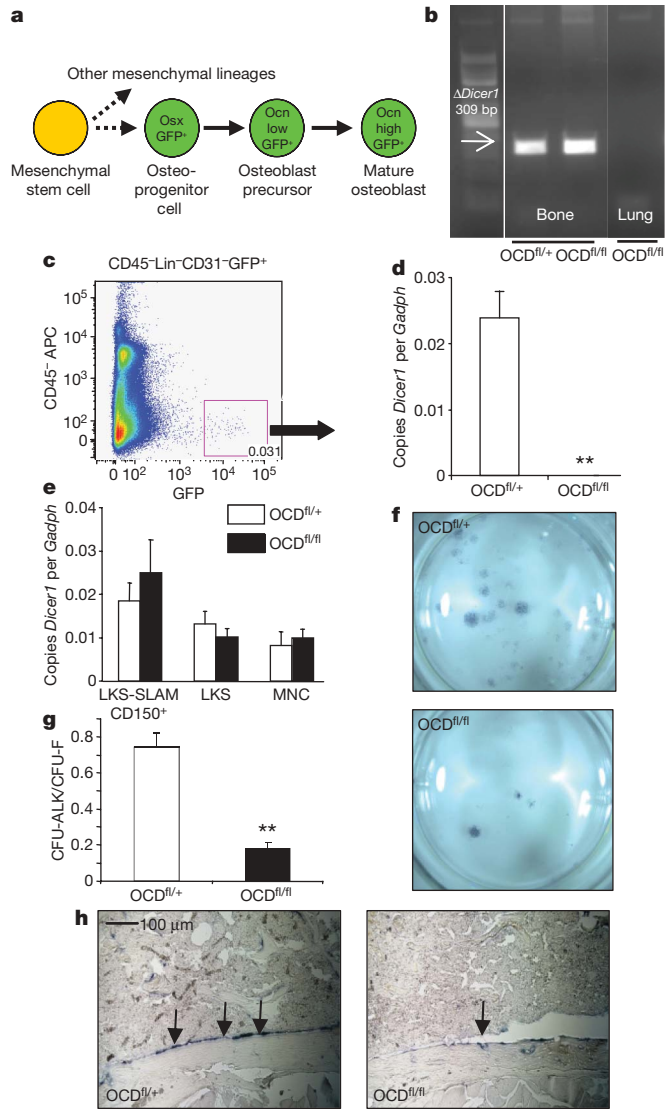


**Figure 1 | Impaired osteoblastic differentiation in OCD$^{fl/fl}$ mice.** **a**, Endogenous osterix (Osx) expression in osteolineage cells. **b–d**, *Dicer1* deletion (Δ) was demonstrated by genomic PCR (**b**) and gene expression of primary osteolineage cells ($n = 5$) (**c**, **d**). APC, allophycocyanin; bp, base pairs. **e**, *Dicer1* gene expression in haematopoietic subsets excluding *Dicer1* deletion from haematopoietic cells in OCD$^{fl/fl}$ mice ($n = 4$). LKS-SLAM, lineage$^-$c-kit$^+$ Sca1$^+$ CD150$^+$ CD48$^-$ cells. MNC, mononuclear cells. **f–h**, Impaired osteogenic differentiation capacity of OCD$^{fl/fl}$ bone marrow stromal cells as shown by reduced CFU-ALK ($n = 2$, performed in quadruplicate) (**f**, **g**), and decreased *osteocalcin* gene expression by *in situ* hybridization (**h**). Arrows in **h** indicate osteocalcin at the endosteal surface. Data in **d**, **e** and **g** are mean ± s.e.m. $^{**}P \leq 0.01$. For further details see Supplementary information.

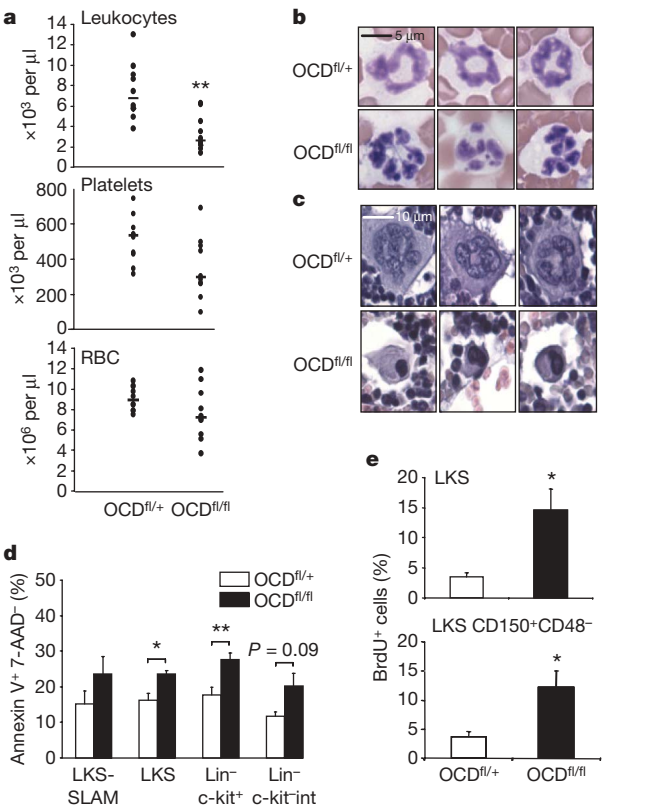


**Figure 2 | Myelodysplasia in OCD$^{fl/fl}$ mice.** **a**, Leukopenia with variable anaemia ($P = 0.16$) and thrombocytopenia ($P = 0.08$) in OCD$^{fl/fl}$ mice ($n = 10$). RBC, red blood cells. **b**, Blood smears showing dysplastic hyperlobulated nuclei in granulocytes. **c**, Bone marrow sections showing micro-megakaryocytes with hyperchromatic nuclei. **d**, Increased apoptosis of haematopoietic progenitor cells in OCD$^{fl/fl}$ mice ($n = 4$). int, intermediate. **e**, Increased proliferation of haematopoietic progenitor cells as shown by *in vivo* bromodeoxyuridine (BrdU) labelling ($n = 4$). Data are mean ± s.e.m. $^*P \leq 0.05$, $^{**}P \leq 0.01$. For further details see Supplementary information.

## Myelodysplasia in OCD$^{fl/fl}$ mice

Leukopenia with reduced numbers of cells in all leukocyte subsets was found in OCD$^{fl/fl}$ mice (Fig. 2a and Supplementary Fig. 2a). Erythrocyte and platelet counts varied widely in OCD$^{fl/fl}$ mice, with some animals showing profound anaemia and thrombocytopenia (Fig. 2a). The variability was at least partly explained by extramedullary haematopoiesis in the spleen (Supplementary Fig. 3), mitigating cytopenia in those animals. The bone marrow of OCD$^{fl/fl}$ mice was normo- to hypercellular (Supplementary Fig. 2b, c). No significant differences were found in the frequency of immunophenotypically defined haematopoietic stem (lineage$^-$c-kit$^+$Sca1$^+$ (LKS) CD150$^+$CD48$^-$) and progenitor (LKS) cells (Supplementary Figs 2d, e and 4). Limiting-dilution transplant analysis showed an increase in HSCs in mutants that did not reach statistical significance (1:29,000 versus 1:52,000, $P = 0.14$). HSC and progenitor function were not impaired in OCD$^{fl/fl}$ mice, as demonstrated by competitive reconstitution capacity after transplantation or colony-forming unit (CFU in culture (CFU-C)) analysis (Supplementary Fig. 2f, g). Decreased blood cell counts despite normal bone marrow cellularity and normal to increased stem cell function is characteristic of ineffective haematopoiesis.

Morphological assessment showed marked dysplasia, with nuclear hypersegmentation in neutrophils and giant platelets in the blood, and micro-megakaryocytes with hypolobulated, hyperchromatic nuclei in the bone marrow of OCD$^{fl/fl}$ mice (Fig. 2b, c and Supplementary Fig. 5a–c). There was neither increased fibrosis on reticulin staining nor ring sideroblasts on iron stains of the bone marrow (not shown). Peripheral cytopenia with dysgranulopoiesis and dysplastic megakaryocytes is consistent with a diagnosis of myelodysplastic syndrome (MDS) in mice according to the Bethesda criteria[12]. The aetiology of human MDS is complex and poorly understood. It has been very difficult to engraft and propagate the haematopoietic characteristics of human MDS in mouse models by transplanting haematopoietic cells from MDS patients into immunodeficient mice, sparking a longstanding debate about a potential causative or facilitating role of the microenvironment in the pathogenesis of this disease.

Examining other principle characteristics of the human disease, we observed increased apoptosis and proliferation of primitive haematopoietic progenitors (Fig. 2d, e and Supplementary Figs 6–8a)[13]. Increased apoptosis was limited to primitive progenitor cells, as no differences were observed in differentiated (lineage$^+$) cells (not shown). Within lineage-c-kit$^+$ cells, apoptosis was most pronounced

in megakaryocyte-erythroid progenitors (MEP) (Supplementary Fig. 7). HSCs are generally more quiescent in close proximity to the endosteal surface *in vivo*[14]. When we imaged transplanted wild-type cells, we noted that LKS cells located significantly closer to the endosteum in mutant animals compared with controls (Supplementary Fig. 8b, c), and the frequency of cell duplets, an indicator of cell proliferation, was markedly increased (Supplementary Fig. 8d), demonstrating increased proliferation of primitive progenitors despite close proximity to the endosteal surface.

$OCD^{fl/fl}$ mice also had reduced B cells and B-cell progenitors, with a concomitant increased frequency of myeloid cells in the bone marrow (Supplementary Figs 2h, i and 9), as observed in human MDS[15,16]. The nature of the B-cell defect in early MDS has remained elusive because cytogenetic studies have failed to link B cells to the malignant clone in MDS. Interestingly, osteoblasts have recently been shown to constitute a niche for B-cell lymphopoiesis[17,18]. $OCD^{fl/fl}$ mice also showed variable, but increased vascularity in the bone marrow, a feature that has been described in MDS[19] (Supplementary Fig. 2j). Deficiencies of either vitamin B12 or folate, which can cause myelodysplastic features[13], were excluded as contributing factors in the $OCD^{fl/fl}$ mice (not shown).

## Myelodysplasia is environmentally induced

Next, we used transplantation to assess the contribution of the microenvironment to the haematopoietic phenotype. Haematopoietic cells of $OCD^{fl/fl}$ (CD45.2) mice demonstrating profound cytopenia and myelodysplastic features were transplanted into B6.SJL (CD45.1) mice ('wild-type environment') (Fig. 3a). Transplanted animals were without apparent signs of disease. The assessment of peripheral blood and bone marrow 16 weeks (Fig. 3a–d and Supplementary Fig. 10) or 12 months (Supplementary Fig. 11) after transplant showed nearly complete donor (CD45.2) chimaerism, with complete normalization of cytopenias, granulocyte and megakaryocyte morphology, intramedullary apoptosis of primitive progenitors and bone marrow vascularity. The results indicate that the haematopoietic phenotype cannot be propagated in a haematopoietic cell-autonomous manner. Conversely, when bone marrow cells from wild-type B6.SJL mice were transplanted into lethally irradiated mutant or control mice (Fig. 3e–h and Supplementary Fig. 12), mutant recipients developed leukopenia, anaemia and thrombocytopenia, dysplastic features of CD45.1 blood cells, increased bone marrow vascularity with dysplastic megakaryocytes, increased frequency of myeloid cells, decreased frequency of B-cell subsets and increased apoptosis of primitive haematopoietic progenitors. The combined experiments provide formal proof that the myelodysplastic phenotype observed in mutant mice is determined by the microenvironment.

## Osteolineage stage specificity

To examine whether mesenchymal cells of the osteoblastic lineage can directly induce aberrant haematopoiesis, we established bone-marrow-derived stromal cell cultures from $OCD^{fl/+}$ versus $OCD^{fl/fl}$ mice and co-cultured these with red-fluorescent (DsRed) haematopoietic LKS and MEP cells (Supplementary Fig. 13). Stromal cells were osteolineage-committed as evidenced by *osterix* expression (and deletion of *Dicer1*; not shown), but lacked terminally differentiated osteoblasts as indicated by the absence of *osteocalcin* expression (Supplementary Fig. 13a). Co-cultures on $osterix^{+}$ $osteocalcin^{-}$ $OCD^{fl/fl}$ stromal cells showed increased proliferation of LKS cells (Supplementary Fig. 13b–d) and impaired megakaryocyte differentiation of MEP cells (Supplementary Fig. 13e–h). The latter was accompanied by morphological changes in megakaryocytic cells (Supplementary Fig. 13i), resembling those observed *in vivo*. Together, the data show

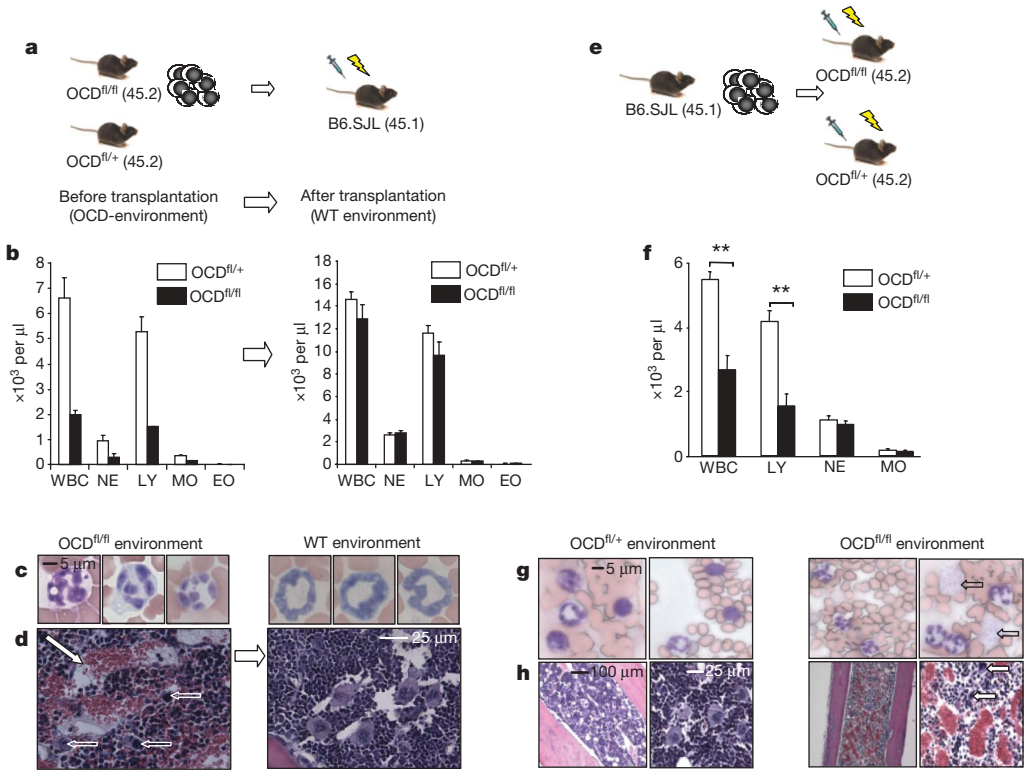


**Figure 3 | Myelodysplasia in $OCD^{fl/fl}$ mice is induced by the bone marrow microenvironment.** **a–d**, Bone marrow cells of $OCD^{fl/fl}$ or littermate $OCD^{fl/+}$ mice ($n = 2$) were transplanted into lethally irradiated wild-tye (B6.SJL) mice ($n = 4$ per OCD mouse) demonstrating complete normalization of leukopenia (**b**), granulocyte (**c**) and megakaryocyte morphology (**d**, open arrows) and bone marrow vascularity (**d**, closed arrow) 16 weeks after transplant. EO, eosinophils; LY, lymphoyctes; MO, monocytes; NE, neutrophils; WBC, white blood cells. **e–h**, Conversely, when wild-type B6.SJL cells were transplanted into $OCD^{fl/+}$ or $OCD^{fl/fl}$ mice ($n = 8$), haematopoiesis in mutant mice at 8 weeks showed leukopenia (**f**), dysgranulopoiesis with giant platelets (**g**, indicated by arrows), and increased bone marrow vascularity with dysplastic megakaryopoiesis (**h**, arrows). Data in **b** and **f** are mean ± s.e.m. $^{**}P \leq 0.01$. For further details see Supplementary information.

that the disruption of haematopoiesis observed in $OCD^{fl/fl}$ mice *in vivo* is, at least partly, the result of a direct effect of $osterix^{+}$ $osteocalcin^{-}$ osteolineage cells on haematopoietic cell proliferation and differentiation. To explore further whether osteoprogenitor cells rather than terminally differentiated ($osteocalcin^{+}$) osteoblasts were the key participants in the haematopoietic abnormality, we crossed $Dicer^{fl/fl}$ with mice in which Cre recombinase was driven by the *osteocalcin* promoter. Efficient recombination by osteocalcin-Cre was confirmed as previously demonstrated[20] (Supplementary Fig. 14a), and serial dilution of DNA isolated from long bones demonstrated equivalent efficacy of *Dicer1* deletion using either the osteocalcin- or osterix-driven Cre (not shown). *Dicer1* deletion in this genetic context recapitulated some aspects of the bone phenotype, notably the altered texture and increased volume of cortical bone (Supplementary Fig. 14b, c), but did not result in any haematopoietic abnormalities (Supplementary Fig. 14d–h). The data demonstrate that osteoprogenitor cell-specific effects of *Dicer1* deletion underlie the disruption of haematopoiesis, and indicate that select subsets of cells in the osteoblast lineage have discrete functions in regulating haematopoiesis.

## Emergence of leukaemia

Human MDS is characterized by transformation to acute myeloid leukaemia in a significant subset of patients. Notably, we observed the infrequent occurrence of myeloblastic tumours in $OCD^{fl/fl}$ mice. Four mice were observed to have facial tumours (estimated frequency 2 out of 100 $OCD^{fl/fl}$ animals), of which three animals were available for detailed analysis (Fig. 4a). Tumours appeared at the age of 2–3 weeks and mice died at age 4–5 weeks. Analyses in a separate cohort of animals demonstrated that dysplastic features were already present in 3-week-old animals (Supplementary Fig. 15), suggesting that tumorigenesis occurred in the context of existing dysplasia. Histological examination of the tumours established a diagnosis of myeloid sarcoma (Fig. 4b), a soft-tissue complication of acute myelogenous leukaemia (AML). *Dicer1* had not been deleted in these myeloid sarcomas as determined by genomic PCR (Fig. 4c). Comparative genomic hybridization to germline DNA showed genetic abnormalities in all tumours, providing direct evidence that the microenvironment facilitated clonal evolution of tumour cells (Fig. 4d and Supplementary Fig. 16). Cytogenetic abnormalities included amplification of a common (27 kilobase (kb)) region on chromosome 14qC1 in two tumours, the biological relevance of which, in the absence of known genes related to tumorigenesis in this region, is under investigation.

The myeloid sarcomas displayed infiltrative behaviour into surrounding tissues (Supplementary Fig. 17) and were diagnosed in a context of myelocytosis (Fig. 4e), anaemia (Fig. 4f), profound splenomegaly with infiltration of blasts (Fig. 4g, h), and a marked increase in blasts with a monocytic appearance in blood and bone marrow (Fig. 4i–k). This combination of findings strongly resembles monoblastic AML (French–American–British (FAB) subtype AML M4/M5) in humans, and fulfilled all criteria for the diagnosis of AML in mice[12]. Although the presence of myeloid sarcoma and acute monocytic leukaemia-like disease in $OCD^{fl/fl}$ mice was sporadic, myeloid sarcomas were never observed in $OCD^{fl/+}$ or Osx-Cre mice (which were fourfold more abundant than mutant animals) and the occurrence of spontaneous AML in mice at age 2–3 weeks is unprecedented to our knowledge. Taken together, these data demonstrate that the disruption of *Dicer1* from cells of the osteoblastic lineage causes myelodysplasia in mice recapitulating important characteristics of human MDS, including the propensity to develop AML.

## Deletion of Shwachman–Diamond–Bodian syndrome gene

To obtain insight into the genes and molecular pathways in osteolineage cells driving the disruption of haematopoiesis in $OCD^{fl/fl}$ mice, we performed gene expression profiling of primary $OCD^{fl/+}$ and $OCD^{fl/fl}$ osteolineage cells ($GFP^{+}CD45^{-}lineage^{-}CD31^{-}$). Microarray analysis showed a broad changes in the transcriptome in $OCD^{fl/fl}$ osteolineage

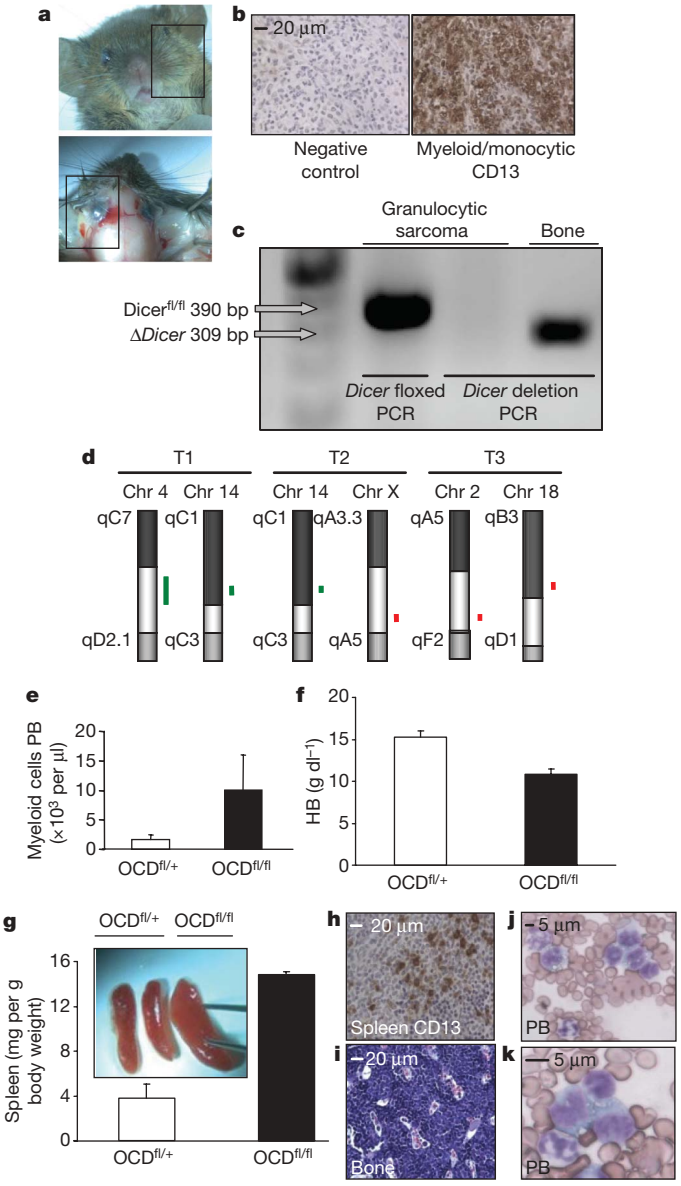


**Figure 4 | Myeloid sarcoma and acute myelogenous leukaemia in $OCD^{fl/fl}$ mice.** **a**, Tumours infiltrating soft tissue in 2–4-week-old mice. Data are from one representative animal. **b**, Tumour sections showing predominantly myeloblasts admixed with maturing granulocytes, typical of myeloid sarcoma and confirmed by immunostaining with CD13. **c**, Exclusion of *Dicer1* deletion in myeloid sarcoma cells by genomic PCR. Bone from the same animal shown as a positive control. **d**, Genomic aberrancies detected in myeloid sarcomas ($n = 3$) as detected by array-based comparative genomic hybridization (CGH). A common amplified region was identified on chromosome (Chr) 14qC1 in two tumours. Green lines represent amplifications, red line represents deletion. **e**, Myelocytosis. PB, peripheral blood. **f**, Anaemia. HB, haemoglobin. Data in **e**–**g** are mean ± s.e.m. **g**–**i**, Splenomegaly, with infiltration of $CD13^{+}$ blasts in the spleen (**h**), and bone marrow (**i**). **j**, **k**, Monocytic blasts in a background of dysplastic granulocytes in the peripheral blood.

cells, with differential expression of 656 genes ($P \leq 0.05$, Student's *t*-test) representing a wide array of functional groups (Supplementary Table 1). Gene set enrichment analysis (GSEA) showed significant enrichment (false discovery rate (FDR) $< 0.05$) of genes involved in early osteoblastic differentiation and commitment[21], including the Wnt–β-catenin[9] and TGF-β signalling pathway[22], in $OCD^{fl/+}$ samples (Supplementary Table 2). Notably, differentially expressed genes and pathways also included stress response genes and cytokines (Supplementary Tables 2 and 3), with significant downregulation of the Shwachman–Diamond–Bodian syndrome (*Sbds*) gene (2.43-fold;

$P = 0.028$, Supplementary Table 1) of particular interest because of its association with human disease. Inactivating mutations in the human *SBDS* gene are highly associated with the clinical syndrome[23] characterized by skeletal abnormalities, bone marrow failure with mild myelodysplastic changes, the propensity to develop MDS and secondary AML, increased intramedullary apoptosis of haematopoietic progenitors, and exocrine pancreatic dysfunction. Studies knocking down the *SBDS* gene in haematopoietic progenitor subsets have failed to recapitulate key features of the clinical phenotype[24], and a role for the bone marrow microenvironment in the pathogenesis of the syndrome has been suggested[25]. Targeted *Sbds* deletion from osteoprogenitor cells by intercrossing osterix-Cre mice to mice containing conditional (floxed) *Sbds* alleles (Fig. 5a) (S.Z. *et al.*, manuscript submitted) resulted in altered texture of the cortical bone (Supplementary Fig. 18a), leukopenia and lymphopenia (but not neutropenia) (Fig. 5b), dysplastic features of neutrophils in the peripheral blood (Fig. 5c), and micromegakaryocytes (Fig. 5d) with increased vascularity of the bone marrow (Fig. 5e). Further similarities with $OCD^{fl/fl}$ mice included decreased frequency of B cells and B-cell progenitors (Supplementary Fig. 18b), increased frequency of myeloid cells (Supplementary Fig. 18c) and intramedullary apoptosis of haematopoietic progenitor cells (Fig. 5f). Collectively, the data show that conditional deletion of *Sbds* from osteoprogenitor cells recapitulates key characteristics of $OCD^{fl/fl}$ mice, and implicate osteoprogenitor cells in the pathogenesis of the Shwachman–Diamond syndrome.

## Discussion

These studies show that specific changes in specific mesenchymal cells of the haematopoietic microenvironment may be sufficient to initiate a complex phenotype of disordered homeostasis with similarities to myelodysplasia, a poorly understood human disease. Furthermore, we demonstrate the ability of this abnormality to result in the emergence of a clonal neoplasm in a cell type of clearly distinct lineage with distinct secondary genetic changes. The data indicate that individual, well-defined, mesenchymal microenvironment constituents can be primary enablers of neoplastic changes in a heterologous cell type.

Although a series of genetic and epigenetic events in a single cell may be necessary for oncogenesis, they may not be sufficient, and a permissive microenvironment has been suggested to be required for frank malignancy to emerge[26]. Examples of microenvironmental contributions to neoplasia include a necessary mast cell contribution to *Nf1*-induced neurofibromas[27] and mesenchymal cell alteration of epithelial tumour growth kinetics[28,29]. Changes in a tissue microenvironment have also been suggested to precede and promote the initiation of genetic events by creating a 'pre-malignant' state characterized by disruption of quiescence-inducing signals or increases in proliferative signalling[30,31]. This has been validated experimentally with altered TGF-β signalling in tissue fibroblasts[32] and with myeloid progenitor expansion after RAR-γ deletion in bone marrow or Rb deficiency in haematopoietic and microenvironmental cells[33,34].

Our findings support the mechanism of malignancy resulting from the interaction of cell autonomous and microenvironmentally determined events, and point to the microenvironment as the site of the initiating event that leads to secondary genetic changes in other cells. It is therefore possible to envision a 'niche-based' model of oncogenesis in which a change in a specific microenvironmental cell can serve as the primary moment in a multi-step process towards malignancy of a supported, but distinct cell type. Signals from the microenvironment may select for subsequent transforming events and therefore such signals may represent candidate therapeutic targets in both treatment and prevention strategies.

Whether osteoprogenitor cell abnormalities are involved in the pathogenesis of human MDS and leukaemia cannot be discerned from our studies. MDS is a heterogeneous disorder in which cytogenetics can be normal or reveal specific clonal lesions such as deletion of 5q. A role for the microenvironment in MDS has been raised, and reduced osteoblast surface and unchanged bone volume similar to our $OCD^{fl/fl}$ model has been reported[35]. Our findings raise the possibility that microenvironmental alterations may precede and facilitate clonal evolution in MDS. Studies examining patient samples will explore this possibility.

The *Sbds* studies provide further suggestive links to human disease. The human syndrome combines features seen in our model and raises the issue of whether both the pathophysiology of the disorder and the difficulty in treating this syndrome with bone marrow transplantation is in part due to a microenvironmental defect in the bone marrow.

The function of *Sbds* is itself unclear, but it has been implicated in ribosomal biogenesis[23] and may therefore share with *Dicer1* the ability to modulate the gene expression 'landscape'. Although we pursued *Sbds* because its expression was decreased in the absence of *Dicer1*, levels in $OCS^{fl/fl}$ are likely to be even lower and as a consequence, may not truly portray the role of *Sbds* in our model. We therefore regard *Sbds* as a candidate participant in the phenotype of $OCD^{fl/fl}$ mice, but further studies will be needed to define the collaborating molecules causing the haematopoietic abnormalities.

These studies were initiated focusing on the stem cell niche, but the results indicate that individual microenvironment constituents can serve as regulators of tissue functions beyond that of stem cell support. Osteoprogenitor dysfunction induced altered proliferation and differentiation of both HSCs and distinct haematopoietic progenitor subsets, and induced changes in the tissue architecture. Within a tissue microenvironment, certain elements may have far broader, integrative functions as the osteoprogenitor cells did here. There may be a hierarchy of activity within niche components as well as the cells they regulate. Our studies provide the rationale for further exploration of the complexity of mesenchymal stroma and the role

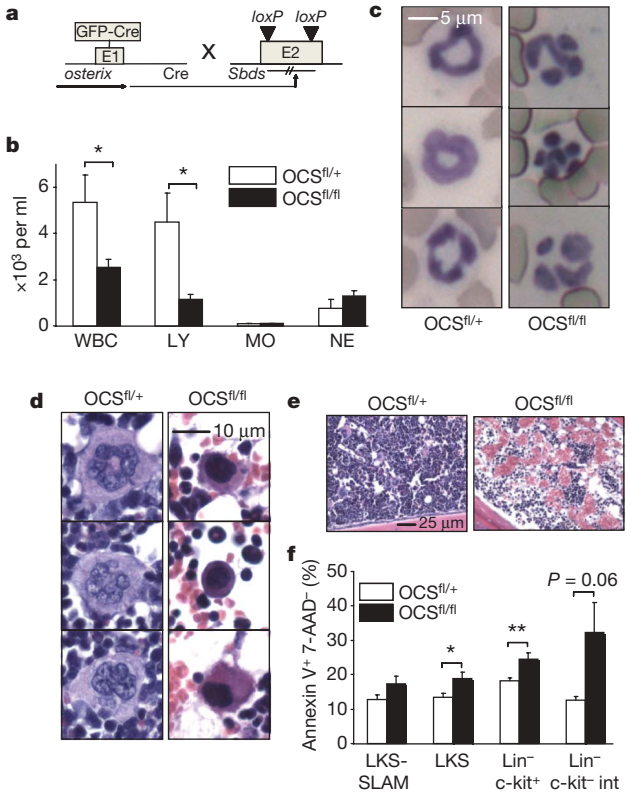


**Figure 5 | Targeted deletion of the *Sbds* gene from osteoprogenitor cells recapitulates many features of the $OCD^{fl/fl}$ phenotype.** **a**, Genetic model of *Sbds* deletion from osteoprogenitor cells. **b**, Leukopenia ($n = 8$). **c**, Dysplasia of neutrophils in peripheral blood. **d**, Dysplasia of megakaryocytes (micromegakaryocytes). **e**, Hypervascularity of the bone marrow. **f**, Increased intramedullary apoptosis of haematopoietic progenitor cells ($n = 5$). Data in **b** and **f** are mean ± s.e.m. $*P \leq 0.05$, $**P \leq 0.01$.

specific mesenchymal subsets may have as primary regulators of normal and disordered tissue function.

## METHODS SUMMARY

**Mice.** Osx-Cre transgenic mice[9], Ocn-Cre transgenic mice[20] and floxed *Dicer1* mice[10], have been described. B6.SJL-*Ptprc*$^{a}$ *Pep3*$^{b}$/BoyJ mice were purchased from the Jackson Laboratory.

**Transplantation.** For competitive transplantation, $5 \times 10^5$ bone marrow cells from 6-week-old OCD$^{fl/+}$ or OCD$^{fl/fl}$ (CD45.2$^+$) littermates admixed with $5 \times 10^5$ CD45.1$^+$ (competitor) wild-type cells were injected into lethally irradiated (9 Gy, split dose) B6.SJL (CD45.1$^+$) mice. For 'wild-type into mutant' experiments, wild-type congenic B6.SJL (CD45.1$^+$) bone marrow cells ($1 \times 10^6$ cells per recipient) were transplanted into lethally irradiated 4-week-old OCD$^{fl/+}$ and OCD$^{fl/fl}$ (CD45.2$^+$) recipients. For 'mutant into wild-type' experiments, OCD$^{fl/+}$ or OCD$^{fl/fl}$ (CD45.2$^+$) were transplanted into lethally irradiated 4-week-old B6.SJL (CD45.1$^+$) animals. Donor cell engraftment was confirmed by FACS.

**Full Methods** and any associated references are available in the online version of the paper at www.nature.com/nature.

**Received 27 February 2009; accepted 19 January 2010.**
**Published online 21 March 2010.**

1. Calvi, L. M. *et al.* Osteoblastic cells regulate the haematopoietic stem cell niche. *Nature* **425,** 841–846 (2003).
2. Zhang, J. *et al.* Identification of the haematopoietic stem cell niche and control of the niche size. *Nature* **425,** 836–841 (2003).
3. Chan, C. K. *et al.* Endochondral ossification is required for haematopoietic stem-cell niche formation. *Nature* **457,** 490–494 (2009).
4. Fleming, H. E. *et al.* Wnt signaling in the niche enforces hematopoietic stem cell quiescence and is necessary to preserve self-renewal in vivo. *Cell Stem Cell* **2,** 274–283 (2008).
5. Bartel, D. P. MicroRNAs: genomics, biogenesis, mechanism, and function. *Cell* **116,** 281–297 (2004).
6. Krol, J. *et al.* Ribonuclease dicer cleaves triplet repeat hairpins into shorter repeats that silence specific targets. *Mol. Cell* **25,** 575–586 (2007).
7. Lu, J. *et al.* MicroRNA-mediated control of cell fate in megakaryocyte-erythrocyte progenitors. *Dev. Cell* **14,** 843–853 (2008).
8. Kumar, M. S. *et al.* Impaired microRNA processing enhances cellular transformation and tumorigenesis. *Nature Genet.* **39,** 673–677 (2007).
9. Rodda, S. J. & McMahon, A. P. Distinct roles for Hedgehog and canonical Wnt signaling in specification, differentiation and maintenance of osteoblast progenitors. *Development* **133,** 3231–3244 (2006).
10. Cobb, B. S. *et al.* T cell lineage choice and differentiation in the absence of the RNase III enzyme Dicer. *J. Exp. Med.* **201,** 1367–1373 (2005).
11. Nakashima, K. *et al.* The novel zinc finger-containing transcription factor osterix is required for osteoblast differentiation and bone formation. *Cell* **108,** 17–29 (2002).
12. Kogan, S. C. *et al.* Bethesda proposals for classification of nonlymphoid hematopoietic neoplasms in mice. *Blood* **100,** 238–245 (2002).
13. Heaney, M. L. & Golde, D. W. Myelodysplasia. *N. Engl. J. Med.* **340,** 1649–1660 (1999).
14. Celso, C. L. *et al.* Live-animal tracking of individual haematopoietic stem/progenitor cells in their niche. *Nature* **457,** 92–96 (2008).
15. Sternberg, A. *et al.* Evidence for reduced B-cell progenitors in early (low-risk) myelodysplastic syndrome. *Blood* **106,** 2982–2991 (2005).
16. van de Loosdrecht, A. A. *et al.* Identification of distinct prognostic subgroups in low- and intermediate-1-risk myelodysplastic syndromes by flow cytometry. *Blood* **111,** 1067–1077 (2008).
17. Zhu, J. *et al.* Osteoblasts support B-lymphocyte commitment and differentiation from hematopoietic stem cells. *Blood* **109,** 3706–3712 (2007).
18. Wu, J. Y. *et al.* Osteoblastic regulation of B lymphopoiesis is mediated by $G_s\alpha$-dependent signaling pathways. *Proc. Natl Acad. Sci. USA* **105,** 16976–16981 (2008).
19. Korkolopoulou, P. *et al.* Prognostic evaluation of the microvascular network in myelodysplastic syndromes. *Leukemia* **15,** 1369–1376 (2001).
20. Zhang, M. *et al.* Osteoblast-specific knockout of the insulin-like growth factor (IGF) receptor gene reveals an essential role of IGF signaling in bone matrix mineralization. *J. Biol. Chem.* **277,** 44005–44012 (2002).
21. Schilling, T. *et al.* Microarray analyses of transdifferentiated mesenchymal stem cells. *J. Cell. Biochem.* **103,** 413–433 (2008).
22. Janssens, K. *et al.* Transforming growth factor-β1 to the bone. *Endocr. Rev.* **26,** 743–774 (2005).
23. Boocock, G. R. *et al.* Mutations in SBDS are associated with Shwachman–Diamond syndrome. *Nature Genet.* **33,** 97–101 (2003).
24. Rawls, A. S. *et al.* Lentiviral-mediated RNAi inhibition of Sbds in murine hematopoietic progenitors impairs their hematopoietic potential. *Blood* **110,** 2414–2422 (2007).
25. Dror, Y. & Freedman, M. H. Shwachman–Diamond syndrome: an inherited preleukemic bone marrow failure disorder with aberrant hematopoietic progenitors and faulty marrow microenvironment. *Blood* **94,** 3048–3054 (1999).
26. Hanahan, D. & Weinberg, R. A. The hallmarks of cancer. *Cell* **100,** 57–70 (2000).
27. Yang, F. C. *et al. Nf1*-dependent tumors require a microenvironment containing *Nf1*$^{+/-}$- and c-kit-dependent bone marrow. *Cell* **135,** 437–448 (2008).
28. Yauch, R. L. *et al.* A paracrine requirement for hedgehog signalling in cancer. *Nature* **455,** 406–410 (2008).
29. Trimboli, A. J. *et al.* Pten in stromal fibroblasts suppresses mammary epithelial tumours. *Nature* **461,** 1084–1091 (2009).
30. Li, L. & Neaves, W. B. Normal stem cells and cancer stem cells: the niche matters. *Cancer Res.* **66,** 4553–4557 (2006).
31. Sneddon, J. B. & Werb, Z. Location, location, location: the cancer stem cell niche. *Cell Stem Cell* **1,** 607–611 (2007).
32. Bhowmick, N. A. *et al.* TGF-β signaling in fibroblasts modulates the oncogenic potential of adjacent epithelia. *Science* **303,** 848–851 (2004).
33. Walkley, C. R. *et al.* A microenvironment-induced myeloproliferative syndrome caused by retinoic acid receptor γ deficiency. *Cell* **129,** 1097–1110 (2007).
34. Walkley, C. R. *et al.* Rb regulates interactions between hematopoietic stem cells and their bone marrow microenvironment. *Cell* **129,** 1081–1095 (2007).
35. Mellibovsky, L. *et al.* Bone remodeling alterations in myelodysplastic syndrome. *Bone* **19,** 401–405 (1996).

**Supplementary Information** is linked to the online version of the paper at www.nature.com/nature.

**Acknowledgements** We thank E. Schipani, E. Attar and H. Kronenberg for advice and discussion, A. McMahon for providing the Osx-Cre mice, J. Fujisaki, D. Wilpitz, M. Ohishi, S. Vallet, M. Churchill and G. Frankl for technical assistance, the Histocore (Endocrine Unit), Flow Core at the Center for Regenerative Medicine, Massachusetts General Hospital (L. Pickett and K. Folz-Donahue), and F. Preffer and D. Dombrowski for assistance with histology and flow-cytometry. We thank D. Machon for help preparing the manuscript and the Cytogenetics Core at Brigham Women/Dana Farber (Y. Xiao and C. Lee) for performing CGH analyses. This work was supported by a Fellowship Award of the Dutch Cancer Society (KWF) and a Special Fellowship Award of The Leukemia & Lymphoma Society to M.H.G.P.R. and grants of the National Institutes of Health, the Harvard Stem Cell Institute and the Ellison Medical Foundation to D.T.S.

**Author Contributions** M.H.G.P.R., S.G. and D.T.S. initiated the study. M.H.G.P.R., S.M. and D.T.S. designed the experiments and analysed the data. M.H.G.P.R. carried out most of the experimental work with the help of S.M., J.A.S., T.K., S.G., E.O.S., S.Z., M.M. and Z.A. B.L.E. and F.A.-S. analysed the microarray results. R.P.H. reviewed bone marrow histology and peripheral blood morphology. C.L. supervised the *in vivo* imaging studies. M.M. and J.M.R. provided materials and discussion. M.H.G.P.R. and D.T.S. wrote the manuscript. D.T.S. directed the research. All authors discussed and commented on the manuscript.

**Author Information** Reprints and permissions information is available at www.nature.com/reprints. The authors declare no competing financial interests. Correspondence and requests for materials should be addressed to M.H.G.P.R. (hraaijmakers@partners.org) or D.T.S. (dscadden@mgh.harvard.edu).

## METHODS

**Mice and genotyping.** Osx-Cre transgenic mice[9], Ocn-Cre transgenic mice[20] and floxed *Dicer1* mice[10], have been described. B6.SJL-*Ptprc*$^{a}$ *Pep3*$^{b}$/BoyJ mice were purchased from the Jackson Laboratory. Floxed *Dicer1* mice were on a mixed C57/B6/J129 background. Other mice strains were on a C57/B6 background. Genotyping of Cre transgenic mice was performed by PCR using primers detecting the *Cre* sequence[36]. The floxed and wild-type *Dicer1* alleles were detected by using primers P1: 5′-AGTGTAGCCTTAGCCATTTGC-3′ and P2: 5′-CTGG TGGCTTGAGGACAAGAC-3′. These primers amplify the region spanning the downstream *loxP* sequence. Deletion of the floxed sequence from the *Dicer1* gene was demonstrated by using primers P1, 28290: 5′-AGTAATGTGAGCAAT AGTCCCAG-3′ and P2, 32050AS: 5′-CTGGTGGCTTGAGGACAAGAC-3′. OCD$^{fl/fl}$ animals were compared to OCD$^{fl/+}$ littermates for the studies described here. The Subcommittee on Research Animal Care of the Massachusetts General Hospital approved all animal work according to federal and institutional policies and regulations.

**RT–PCR.** RNA extraction, real-time quantitative PCR with reverse transcription (RT–PCR) and relative gene expression quantification was performed on sorted cells (GFP$^{+}$CD45$^{-}$CD31$^{-}$lineage$^{-}$) as described previously[37] using the following primers: *Dicer1*-F, 5′-AATTGGCTTCCTCCTGGTTAT-3′ and *Dicer1*-R, 5′-GTCAGGTCCTCCTCCTCCTC-3′; *osteocalcin*-F, 5′-CTGACCTCACAG ATCCCAAGC-3′ and *osteocalcin*-R, 5′-TGGTCTGATAGCTCGTCACAAG-3′; *Gapdh*-F, 5′-AGGTCGGTGTGAACGGATTTG-3′ and *Gapdh*-R, 5′-TGTA GACCATGTAGTTGAGGTCA-3′.

**Isolation and osteogenic differentiation of bone-marrow-derived stromal cells.** Mice were euthanized; tibiae, femurs and spine were removed and excess soft tissue was eliminated. Using a pestle and mortar, the bones were crushed and washed in PBS with 0.5% FBS and passed through a 40-μm filter into a collection tube. Cells were spun at 1,500 r.p.m. for 5 min; the supernatant was removed, and cells were resuspended in a minimal volume of ACK lysing buffer (Cambrex) for 4 min on ice and washed once with PBS. After pelleting once again, the cells were resuspended and plated in αMEM, 20% FBS (HyClone), and penicillin and streptomycin solution (CellGro), referred to as αMEM20%, and incubated at 33 °C with 5% $CO_2$. After 3 weeks of culture and expansion, plastic adherent cells were CD45-depleted by magnetic isolation (Invitrogen; Dynabeads Streptavidin) using an anti-mouse CD45 biotin antibody (BD Bioscience; 550539). The plastic adherent CD45-negative cells were then maintained in αMEM20% as before. To assess osteogenic differentiation, bone-marrow-derived stromal cells (passage 3) were plated at $10 \times 10^3$ cells per well in a 96-well plate (BD Biosciences) at 33 °C in osteogenic induction medium: α20% modified with glycerol 2-phosphate (2.16 mg ml$^{-1}$), 2-phospho-L-ascorbic acid (0.05 mg ml$^{-1}$), and dexamethasone (10 nM) (Sigma-Aldrich). After 7 days of differentiation, alkaline phosphatase staining was carried out with BCIP/NBT solution (Sigma-Aldrich) per the manufacturer's instructions. For the von Kossa assay and staining, cells were fixed and washed in water, and a 5% silver nitrate solution was added to the well under incandescent light for 20–45 min. After granules developed, the silver nitrate was removed and wells were washed with water to stop the reaction.

**CFU-F and CFU-ALK.** Five-hundred-thousand primary bone marrow cells were plated in 12-well plates in αMEM20% for the CFU-F assay or osteogenic medium for the CFU-ALK assay. Medium was changed at 24 h to eliminate non-adherent cells. After 7 days, colonies were assessed by methylene blue staining for the CFU-F assay or BCIP staining (alkaline phosphatase) for the CFU-ALK assay.

**Histomorphometric analysis.** Bones were fixed in 4% paraformaldehyde and undecalcified sections embedded in methyl methacrylate resin. Five-micrometre sections were stained with Masson's Trichrome or were left unstained, and histomorphometric analysis was performed with the Osteomeasure system (Osteometrics) using standard procedures. Tibial sections were measured in the proximal metaphysis beginning 340 μm below the chondro-osseous junction. Osteoblasts were identified as mononuclear cells directly abutting either mineralized bone or osteoid and restricted to the endosteal surface.

***In situ* hybridization.** *In situ* hybridization was carried out as described[36]. Complementary $^{35}$S-labelled riboprobes were transcribed from the plasmids encoding mouse *osteocalcin* using Riboprobe systems from Promega. Probes for *osteocalcin* were described[36].

**Haematological measurements.** Peripheral blood samples were obtained by lateral tail vein bleeding. Peripheral blood cell counts were performed on a HEMAVET Multispecies Hematology Analyser (CDC Technologies).

**Methylcellulose colony formation assay.** Bone marrow or spleen cells ($10 \times 10^3$) were plated into methylcellulose (StemCell Technologies) in a 6-well plate and grown for 10 days before being scored.

**FACS analysis.** Haematopoietic progenitors were identified based on their expression of lineage markers as well as c-Kit, Sca1, CD48 and CD150 expression. Lineage staining used a cocktail of biotinylated anti-mouse antibodies to Mac-1α (CD11b), Gr-1(Ly-6G and Ly-6C), Ter119 (Ly-76), CD3, CD4, CD8a (Ly-2), and B220 (CD45R; BD Biosciences). For detection we used streptavidin conjugated with peridinin-chlorophyll-protein complex (PerCP), c-Kit-APC (CD117), CD48-pacific blue (CD135) and CD150-PE-Cy7 (all from BD Biosciences) and Sca1-PE-Cy5.5 (Ly 6A/E; Caltag Laboratories). For congenic strain discrimination, anti-CD45.1–PE (phycoerythrin) and anti-CD45.2–FITC (fluorescein isothiocyanate) antibodies (BD Biosciences) were used. For the apoptosis assay, we used 7-AAD and AnnexinV-APC (BD Biosciences) in combination with streptavidin–PE and c-Kit–FITC (both Biolegend). For the intracellular detection of BrdU–FITC, bone marrow cells were fixed and permeabilized using BD Cytofix/Cytoperm Fixation/Permeabilization Solution Kit (BD Biosciences) according to the manufacturer's recommendations. Compensation and data analysis were performed using Flowjo 8.5.3

**FACS of osteolineage cells.** Whole bone marrow and bone cells were collected by crushing tibias and femurs of mice, stained with biotin-conjugated lineage cocktail antibodies and subjected to lineage depletion using magnetic isolation (Invitrogen; Dynabeads Streptavidin). The resulting lineage-depleted fraction was stained with lineage and CD31-biotin-streptavidin APC-Cy7 (BD Biosciences) and CD45-APC (eBioscience) and sorted using FACS DiVa or FACS ARIA (Becton Dickinson). A small fraction of the collected cells was re-run through the sorter and more than 95% purity was consistently confirmed.

**Collagenase treatment of bone for PCR.** Collagenase digestion was preformed on the bone fragments left in the mortar and 70-μm filter after crushing long bones. A solution of DMEM (Cellgro), 0.2% collagenase (WAKO) and 10 mM HEPES (Fisher) was warmed to 37 °C. In a centrifuge tube, bone fragments were added to the collagenase solution and kept at 37 °C for 90 min, vortexing every 15–30 min. Excess PBS was added to the slurry, which was then filtered through a 40-μm filter. The flow-through was then pelleted.

**Bone marrow histology and peripheral blood morphology.** For histological analysis, long bones were dissected, fixed in paraformaldehyde 4%, decalcified in 10% EDTA, paraffin-processed, cut, and subjected to haematoxylin and eosin staining. Peripheral blood smears were formalin-fixed for 5 min, stained with May-Grunwald (Sigma-Aldrich) for 5 min, rinsed in distilled water with PBS and in Giemsa stain (Sigma-Aldrich) for another 30 min. Permount (Fisher Scientific) was used to mount the sections. Images were acquired with a Nikon Eclipse 80i epifluorescence microscope equipped with a Qimaging Micropublisher digital CCD colour camera. Bone and bone marrow histology was assessed by two independent investigators blinded to mice genotypes.

**Bone marrow transplantation.** All bone marrow transplantations were performed by retro-orbital venous plexus injection. For competitive transplantation, $5 \times 10^5$ whole bone marrow cells from 6-week-old OCD$^{fl/+}$ or OCD$^{fl/fl}$ (CD45.2$^{+}$) littermates were mixed with $5 \times 10^5$ CD45.1$^{+}$ (competitor) wild-type cells and injected into lethally irradiated (9 Gy, split dose on the day of transplant) recipient B6.SJL (CD45.1$^{+}$) mice. Engraftment efficiency in recipients was monitored by donor contribution of CD45.2$^{+}$ cells using FACS analysis. For limiting dilution assays, $2 \times 10^5$, $5 \times 10^4$, $1 \times 10^4$ and $0.5 \times 10^4$ OCD$^{fl/+}$ or OCD$^{fl/fl}$ mononuclear bone marrow cells were mixed with $2 \times 10^5$ wild-type bone marrow cells and injected into lethally irradiated recipients (nine mice per cell dose per genotype). Engraftment efficiency in recipients was monitored by donor contribution of cells using FACS analysis. The frequencies of competitive repopulating units were calculated using the L-Calc software. More than or equal to 1% donor cells in both myeloid and lymphoid lineages was used to determine whether an animal had a positive engraftment. For wild-type into mutant experiments, wild-type congenic B6.SJL (CD45.1$^{+}$) bone marrow cells ($1 \times 10^6$ cells per recipient) were transplanted into lethally irradiated 4-week-old OCD$^{fl/+}$ and OCD$^{fl/fl}$ (CD45.2$^{+}$) recipients. Complete donor cell engraftment by wild-type CD45.1$^{+}$ cells was confirmed by FACS. Conversely, for mutant into wild-type experiments, OCD$^{fl/+}$ or OCD$^{fl/fl}$ (CD45.2$^{+}$) were transplanted into lethally irradiated 4-week-old B6.SJL (CD45.1$^{+}$) animals. Complete donor cell engraftment by CD45.1/CD45.2$^{+}$ cells was confirmed by FACS.

**Immunohistochemistry.** For immunohistochemistry, antigen retrieval was carried out with proteinase K (20 mg ml$^{-1}$, Roche), followed by 3% $H_2O_2$ treatment to block endogenous peroxidase. The TSA Biotin system (PerkinElmer) was used according to the manufacturer's instructions. Specimens were incubated with mouse anti-CD31 antibody (BD Biosciences) or anti-CD13 antibody (Santa Cruz Biotechnology) for 1 h at room temperature.

**BrdU labelling and detection.** Mice received 150 l BrdU solution (10 mg ml$^{-1}$) by intraperitoneal injection. After 15 h, bone marrow was collected for flow cytometric detection of BrdU–FITC uptake according to the manufacturer's instructions (FITC-BrdU Flow kit; BD Biosciences).

***In vivo* imaging.** *In vivo* imaging has been extensively described elsewhere[14]. In brief, $1–5 \times 10^5$ wild-type (B6.SJL) LKS cells were stained with 5 M DiD (1,1′-dioctadecil-3,3,3′-tetramethylindodicarbocyanide perchlorate) in PBS without serum for 10 min at 37 °C, washed once in PBS and immediately injected

into the tail vein of recipient mice. Mice were anaesthetized and prepared for *in vivo* imaging as described. Immediately before imaging, 20 l of non-targeted Qdot 800 or 655 (Invitrogen) diluted in 130 l sterile PBS was injected retro-orbitally to allow vasculature visualization. All mice were imaged with a custom-built confocal two-photon hybrid microscope specifically designed for live animal imaging. Microscopy and image processing have been described. Images were coloured and merged using Adobe Photoshop and LKS-microenvironment distance measures were obtained using Adobe Illustrator and Microsoft Excel. A two-tailed type 2 *t*-test was applied to all data. $P \leq 0.05$ was considered statistically significant.

**Co-culture studies.** Bone marrow stromal cells were isolated and CD45-depleted by magnetic isolation upon confluence and expanded for another week. The expanded cells were then plated at 1,750 cells per well in 384-well tissue culture plates coated with fibronectin (Millipore) in either αMEM20% or osteogenic induction media. After 4 days of culture, 200 LKS or MEP (lineage$^-$, CD127$^-$Sca1$^-$c-kit$^+$CD34$^-$CD16/32$^-$ cells) cells from 8–12-week-old Actin-DsRed positive mice (Jackson Laboratory; 005441) were added to each well. Co-culture was performed without any cytokines. After 7 days of co-culture the number of DsRed cells was assessed by automated microscopy. Megakaryocytes were quantified morphologically as large cells with prominent multinucleated megakaryons (the identity of these cells was also confirmed by CD41 staining).

**Comparative genomic hybrydization.** Direct amplification of DNA from paraformaldehyde-fixed paraffin-embedded (FFPE) tissue samples was performed using a REPLI-g FFPE kit (Qiagen) following the manufacturer's instructions. In brief, FFPE samples were incubated at 95 °C for 10 min followed by lysis at 60 °C for 60 min and ligation at 24 °C for 30 min. Amplification took place at 30 °C for 2 h. Agilent genomic DNA labelling kit was used for the amplified FFPE DNA labelling and purification. For each 244 K array, 2 μg of FFPE DNA and 2 μg of germline reference DNA were labelled with Cy5 and Cy3, respectively. Labelled FFPE DNA and reference DNA were combined and mixed with Cot-1 DNA, blocking agent and hybridization buffer. After denaturation at 95 °C for 3 min and incubation at 37 °C for 30 min, the hybridization mix was loaded onto a gasket slide in an Agilent Surehyb chamber. The array slide was placed on top the gasket slide. The SureHyb chamber was covered, clamped and incubated in a rotator rack in a 65 °C oven for 40 h. In an ozone-controlled environment, hybridized arrays were disassembled, and washed in Agilent Oligo aCGH wash buffer 1 for 5 min, in wash buffer 2 for 1 min at 37 °C, and immediately scanned using an Agilent DNA microarray scanner. Data extraction was conducted using the feature extraction software. Finally, data files were analysed using the Agilent DNA analytics software.

**Oligonucleotide microarrays.** RNA was isolated from sorted GFP$^+$CD45$^-$ CD31$^-$lineage$^-$ cells by Trizol extraction (Invitrogen) according to the manufacturer's protocol. Up to four mice were pooled per sample. Linear amplification of 20 ng total RNA was performed using the Ovation Biotin RNA Amplification and Labelling System (Nugen). The biotinylated cRNA was hybridized to the Affymetrix Mouse430 v2 chip. Signal normalization was performed by the robust multiarray averaging (RMA) method. Data of three samples of OCD$^{fl/fl}$ cells versus three samples of OCD$^{fl/+}$ cells was analysed using GEPAS package[38]. A *t*-test was carried to identify probes differentially expressed between OCD$^{fl/+}$ and OCD$^{fl/fl}$ samples. Gene set enrichment analysis was performed as described[39]. The signal-to-noise metric and permutation of gene sets was used to rank the genes and calculate significance and FDR values. Analysis was performed by collapsing probe sets to unique gene symbols and used to interrogate an established collection of curated gene sets provided by the Molecular Signatures Database (MsigDB, http://broad.mit.edu/gsea/msigdb). The osteogenic gene expression signature was collected from the literature[21] and used to interrogate the gene expression data set comparing OCD$^{fl/+}$ and OCD$^{fl/fl}$ samples for gene set enrichment.

**Statistical analysis.** In all cases, analysis was performed by a standard unpaired, two-tailed Student's *t* test. All data have been plotted as mean ± s.e.m. Statistical significance is indicated by $*P \leq 0.05$ or $**P \leq 0.01$.


36. Kobayashi, T. *et al.* Dicer-dependent pathways regulate chondrocyte proliferation and differentiation. *Proc. Natl Acad. Sci. USA* **105**, 1949–1954 (2008).
37. Raaijmakers, M. H. *et al.* Quantitative assessment of gene expression in highly purified hematopoietic cells using real-time reverse transcriptase polymerase chain reaction. *Exp. Hematol.* **30**, 481–487 (2002).
38. D. Montaner, *et al.* Next station in microarray data analysis: GEPAS. *Nucleic Acids Res.* **34**, W486–W491 (2006).
39. Subramanian, A. *et al.* Gene set enrichment analysis: a knowledge-based approach for interpreting genome-wide expression profiles. *Proc. Natl Acad. Sci. USA* **102**, 15545–15550 (2005).